Calculation of hydrogen and helium concentrations for CSNS target *

Dong-Dong Pan(潘冬冬)[1,2,3] Tai-Ran Liang(梁泰然)[2,4] Wen Yin(殷雯)[2;1)] Ze-En Yao(姚泽恩)[1]

[1] School of Nuclear and technology, Lanzhou University, Lanzhou 730000, China
[2] Spallation Neutron Source Engineering Center for Target and Instrument, Beijing National Laboratory for Condensed Matter Physics, Institute of Physics, Chinese Academy of Science, Beijing 100190, China
[3] Dongguan Branch, Institute of High Energy Physics, Chinese Academy of Sciences, Beijing 100049, China
[4] School of Physics and Electronic Information, Inner Mongolia University for the Nationalities, Tongliao 028043, China

Abstract: The China Spallation Neutron Source (CSNS) is driven by protons whose energies are about 1.6 GeV. At such high energies, the spallation neutrons lead to the formation of large amounts of helium, hydrogen and new heavier species in the form of transmutation products. These hydrogen, helium and transmutation products have a critical effect on the mechanical properties on the one hand and exacerbate the displacement radiation damage on the other hand. In this paper, the background hydrogen/helium concentrations and the maximum hydrogen/helium concentrations near cracks in a tungsten target for CSNS have been calculated at temperatures of 100℃ and 300℃ by applying a theoretical model. For the CSNS tungsten target plate, we find the maximum hydrogen concentration near the tips of cracks ranges from 3.0×10^{-2}–2×10^{-1}, which exceeds the hydrogen background concentration by 1.2–1.8 times; the maximum helium concentration near the tips of cracks ranges from $3.0\times10^{-4}-1.2\times10^{-3}$, which exceeds the helium background concentration by $2-4$ times; the maximum hydrogen/helium concentration increases with the increase of the transfer length across the surfaces of the target and it decreases with the increase of temperature.

Keywords: CSNS, hydrogen concentration, helium concentration, tungsten target

PACS: 29.25.Dz, 61.80.Hg **DOI:** 10.1088/1674-1137/40/3/037004

1 Introduction

A spallation source is an accelerator-based facility to produce high intensity neutron by high energy protons bombarding heavy-metal targets. The China Spallation Neutron Source (CSNS) is currently under construction in Dongguan, China. It can provide 1.6 GeV protons at a 25 Hz repetition rate, with a beam power of 100 kW in phase I, which can be upgraded to 500 kW in phase II. The target material of CSNS is tungsten, which has a high neutron yield. Tungsten has a problem, however, in that the corrosion resistance is poor. To solve this, every tungsten plate target in CSNS is cladded with tantalum. Table 1 shows the main basic parameters and technical indices of CSNS [1].

In spallation source environments, nuclear reactions make up the main part of radiation damage, and produce many foreign elements such as hydrogen and helium. Hydrogen accumulations in the material will build up high hydrogen concentrations which induces hydrogen embrittlement. Recent experiments led to the conclusion that an increase in the ductile-brittle transition temperature (DBTT) due to helium has been found and there is a linear relationship between ΔDBTT and helium concentration for steel irradiated over the range from 2.5 to 18.4 dpa and from 85 to 1530 appm helium [2,3]. Those two types of degradation result in significant decrease of the ductility of materials, creep breaking time and fatigue life.

Table 1. Main parameters and technical indices of CSNS target.

project phase	I	II
proton power/kW	100	500
proton energy/GeV	1.6	1.6
proton current/μA	62.5	315
repetition rate/Hz	25	25
target material	tungsten	
cladding material	tantalum	
target cross section	170 mm×70 mm	
proton beam distribution	Gaussian distribution	
maximum surface temperature of the target	⩽130 ℃	
maximum center temperature of the target	⩽300 ℃	

Received 19 June 2015, Revised 13 October 2015
∗ Supported by National Science Foundation of China (51371195, 11174358)
1) E-mail: wenyin@iphy.ac.cn

Because of the significant role of helium and hydrogen in irradiated metals, especially for spallation neutron source and fusion materials, there are extensive theoretical works on tungsten, iron and zirconium alloys based on density functional theory [4–7]. In this paper, the hydrogen and helium concentrations in target materials for CSNS are calculated based on the diffusion continuity equation and Fick's second law. Firstly, starting from the hydrogen and helium production rate, we obtain the hydrogen and helium background concentration of tungsten plates. Then, in order to study the maximum hydrogen and helium background concentration due to stress-driven hydrogen and helium accumulation, we calculate the enhancement of hydrogen and helium concentration near a crack. Finally, the relationship between the hydrogen and helium concentration and the operating temperature are discussed.

2 Methods and results

2.1 Hydrogen/helium production rate

The following calculations are based on the main parameters shown in Table 1. Here the proton beam power and energy are 500 kW and 1.6 GeV, respectively. The proton beam, which has a Gaussian distribution, bombards a tungsten target which has a cross section shape 170 mm long and 70 mm wide. So we can calculate that the average proton flux is $\Phi_{\rm p}$=1.95×10^{18}m$^{-2}\cdot$s^{-1}, and after assuming an average of 30 neutrons per 1.6 GeV proton generated by spallation reactions, the average neutron flux will be $\Phi_{\rm n}$=5.85×10^{19}m$^{-2}\cdot$s^{-1}. The hydrogen and helium production cross sections $\sigma_{\rm H}$ and $\sigma_{\rm He}$ of tungsten under the spallation energy 1.6 GeV are from FLUKA [8,9] simulation. The computational results are listed in Table 2.

Table 2. Physical data used in the calculations.

tungsten target	
average proton flux	$\Phi_{\rm p}$=1.95×10^{18} m$^{-2}\cdot$s^{-1}(Section 2.1)
average neutron flux	$\Phi_{\rm n}$=5.85×10^{19} m$^{-2}\cdot$s^{-1}(Section 2.1)
hydrogen reaction cross-section	$\sigma_{\rm H}$=4.87×10^{-28} m^2
hydrogen production rate	P=2.94×10^{-8} s^{-1}
hydrogen diffusion coefficient	$D_{\rm eff}$(100℃)=5.45×10^{-11} m$^2\cdot$s^{-1}[10]
	$D_{\rm eff}$(300℃)=3.10×10^{-10} m$^2\cdot$s^{-1}[10]
hydrogen relaxation volume	ΔV =2.57×10^{-30} m^3
helium reaction cross-section	$\sigma_{\rm He}$=1.21×10^{-28} m^2
helium production rate	P=7.31×10^{-9} s^{-1}
helium diffusion coefficient	$D_{\rm eff}$(100℃)=6.14×10^{-9}m^{2}s^{-1}[11]
	$D_{\rm eff}$(300℃)=1.14×10^{-8} m^{2}s^{-1}[11]
helium relaxation volume	ΔV =6.79×10^{-30} m^3
tensile flow stress	$\sigma_{\rm F}$(100℃)=550 MPa
	$\sigma_{\rm F}$(300℃)=440 MPa
poisson ratio	v=0.28

In order to verify the accuracy of the simulation results, we compare the calculated helium production cross section of tungsten when the incident proton is 0.75 GeV with experimental data. The calculated result of 628 mb agrees with the experimental result 762 mb at the error level of 20% [12]. Because proton and neutron-induced hydrogen and helium production cross-sections in tungsten are comparable at 1.6 GeV [13], these results can be expected to apply to either type of projectile. Then the average hydrogen/helium production rate can be obtained according to Eq. (1):

$$\begin{cases} P_{\rm H} = \sigma_{\rm H}\Phi_{\rm p} + \sigma_{\rm H}\Phi_{\rm n} \\ P_{\rm He} = \sigma_{\rm He}\Phi_{\rm p} + \sigma_{\rm He}\Phi_{\rm n} \end{cases}. \tag{1}$$

The results are shown in Table 2.

2.2 Hydrogen/helium background concentration

We consider the target is an infinite metallic plate of thickness 2d. On the condition that high energy protons bombard the target, according to Fick's second law, the average hydrogen/helium concentration $c(z,t)$ inside the plane satisfies the continuity equation

$$D_{\rm eff}\frac{\partial^2 c}{\partial z^2} + P = \frac{\partial c}{\partial t}, \tag{2}$$

where $D_{\rm eff}$ is the effective diffusion coefficient; z denotes a Cartesian axis normal to the surfaces of the plane, its origin at the center of the plate, i.e. in the center of the plane, z=0; t means time and P means hydrogen/helium production rate. Figure 1 shows the values of hydrogen and helium $D_{\rm eff}$ in tungsten [10,11]. In the case of zero

hydrogen/helium partial pressure outside the plate, the boundary conditions are

$$\pm vc = -D_{\rm eff}\frac{\partial c}{\partial z}, \tag{3}$$

where v is the velocity of hydrogen/helium atoms across the surfaces of the plate [14].

When $t \to \infty$, the average hydrogen/helium concentration $c(z,t)$ reads

$$c(z,\infty) = \frac{Pd^2}{2D_{\rm eff}}\left(1+\frac{2l}{d}-\left(\frac{z}{d}\right)^2\right), \tag{4}$$

where $l = D_{\rm eff}/v$ denote the transfer length associated with atom loss across the surfaces of the plate [14]; l=0 means instantaneous outflow, such as an ideal clean surface; $l > 0$ means inhibited flow, like for real contaminated surfaces. l/d is a dimensionless ratio, known as the inverse Hobson number [15]. This parameter characterizes the diffusion resistance of the surface of the tungsten target plate relative to the target plate itself. When $z = 0$, the maximum hydrogen/helium concentration in the center of the plate is given by Eq. (5).

$$c_0 = \frac{Pd^2}{2D_{\rm eff}}\left(1+\frac{2l}{d}\right). \tag{5}$$

Figure 2 shows the steady-state average hydrogen/helium concentration as a function of the plate half-thickness d at two temperatures and two values of l. From Fig. 2, we note that hydrogen/helium background concentration decreases with increasing temperature for both ideal clean and real surfaces; however, the hydrogen/helium background concentration is much higher for a real surface than that for a clean surface.

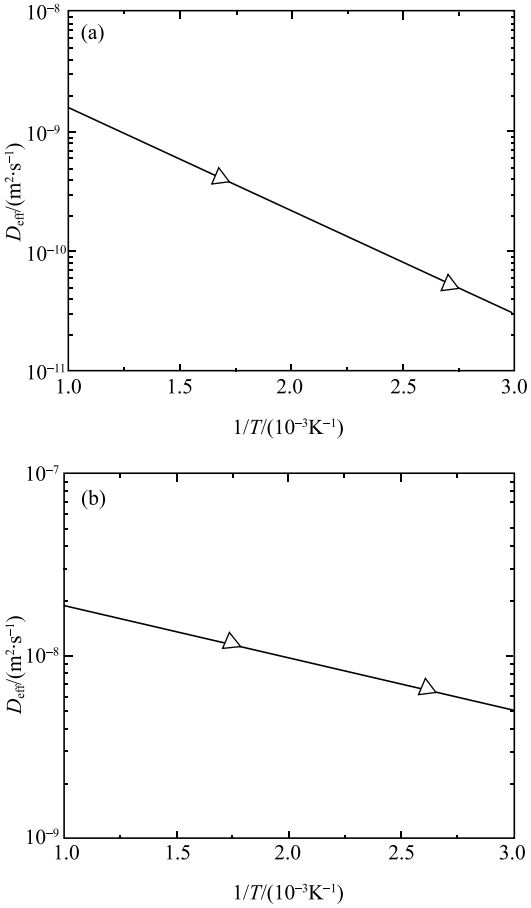

Fig. 1. Effective diffusion coefficient, $D_{\rm eff}$, as a function of inverse absolute temperature $1/T$. (a) $D_{\rm eff}$ of hydrogen in tungsten; (b) $D_{\rm eff}$ of helium in tungsten. The solid triangles denote the data used in this work.

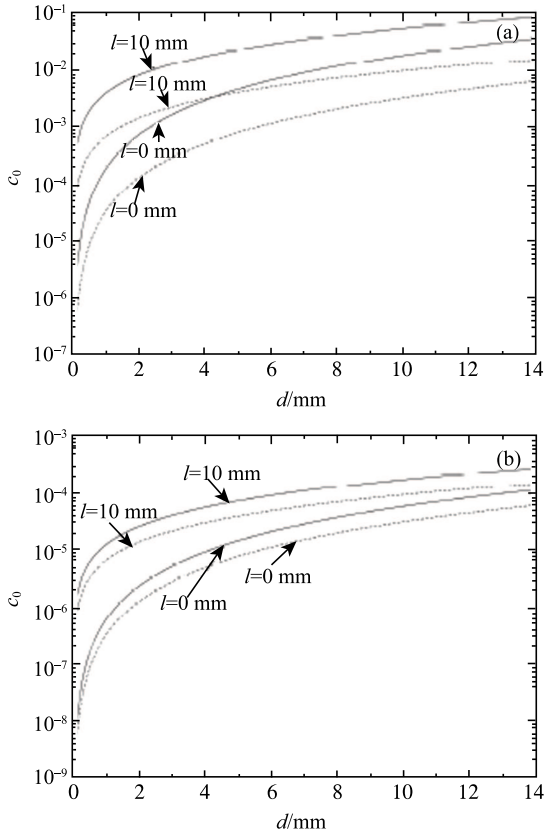

Fig. 2. The hydrogen/helium background concentration in the center of the tungsten plate, as a function of d, (the plate half-thickness), at two different temperature of 100℃ (solid line) and 300℃ (dotted line), for different values of the transfer length l. (a) hydrogen background concentration; (b) helium background concentration.

In this system, the relaxation time of build-up of the steady-state average of hydrogen/helium concentration from zero concentration is [16]

$$\tau_{\rm r} = 1/\lambda^2 D_{\rm eff}, \tag{6}$$

with

$$\lambda l = \cot \lambda d, \tag{7}$$

and by the smallest root of the transcendental relation

$$\tau_{\rm r} \approx \begin{cases} \left(1+\dfrac{l}{d}\right)^2 \tau_0 \left(\text{if}\,\dfrac{l}{d} \ll 1\right) \\ \left(\dfrac{1}{3}+\dfrac{l}{d}\right)\dfrac{\pi^2\tau_0}{4} \left(\text{if}\,\dfrac{l}{d} \gg 1\right) \end{cases}, \tag{8}$$

with

$$\tau_0 = \frac{4d^2}{\pi^2 D_{\rm eff}}. \tag{9}$$

According to Eq. (8), the dependence of relaxation time on l/d is displayed in Fig. 3. In Fig. 3, we note there is a reduction of the relaxation time at a higher temperature, but at the same temperature, the relaxation time will increase with the increase of plate half-thickness d.

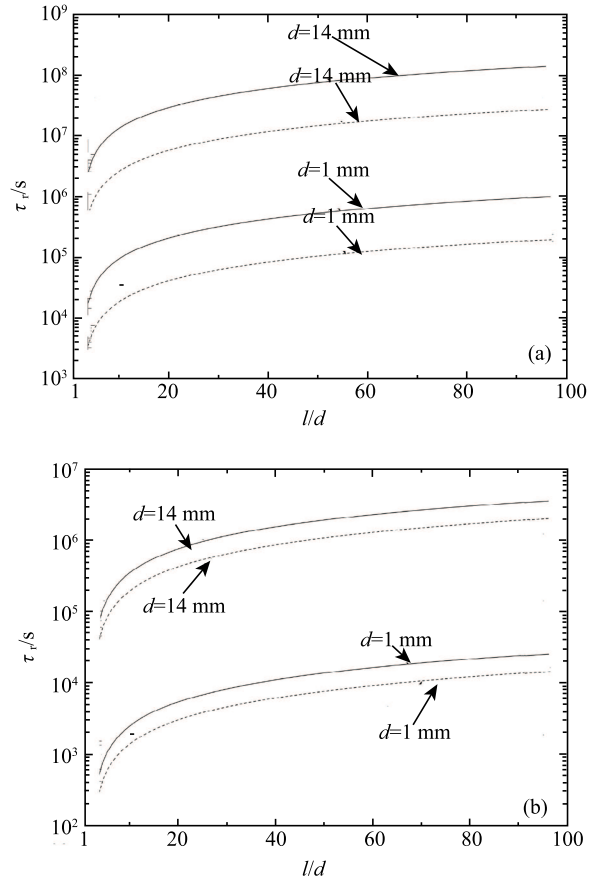

Fig. 3. Relaxation time, as a function of the inverse Hobson number l/d, at two different temperatures, 100℃ (solid line) and 300℃ (dotted line), in the case of d=1 mm and d=14 mm. (a) relaxation time of hydrogen in tungsten; (b) relaxation time of helium in tungsten.

2.3 Hydrogen/helium background near a crack

In this section, we consider a series of straight microcracks of length $2a$, embedded in the center of a plane which is an isotropic elastic/ideally plastic continuum. These microcracks are surrounded by a hydrogen/helium solution of fractional concentration c_0. An external tensile stress $\sigma_{\rm ext}$ is applied perpendicular to the microcrack, as depicted in Fig. 4(a). Obviously these microcracks will increase loading due to hydrogen/helium accumulation in the vicinity of the crack-tip region.

The microcrack length $2a$ is much smaller than the thickness of the plate $2d$, so the length of the crack is negligible, therefore local cylindrical polar coordinates (r,θ) can be used to describe their origin at the crack-tip. The principal components of the tensor of elastic stress σ in the near-field region of radius $r_{\rm K}$ outside the plastic zone can describe the stress field near a crack-tip [17]:

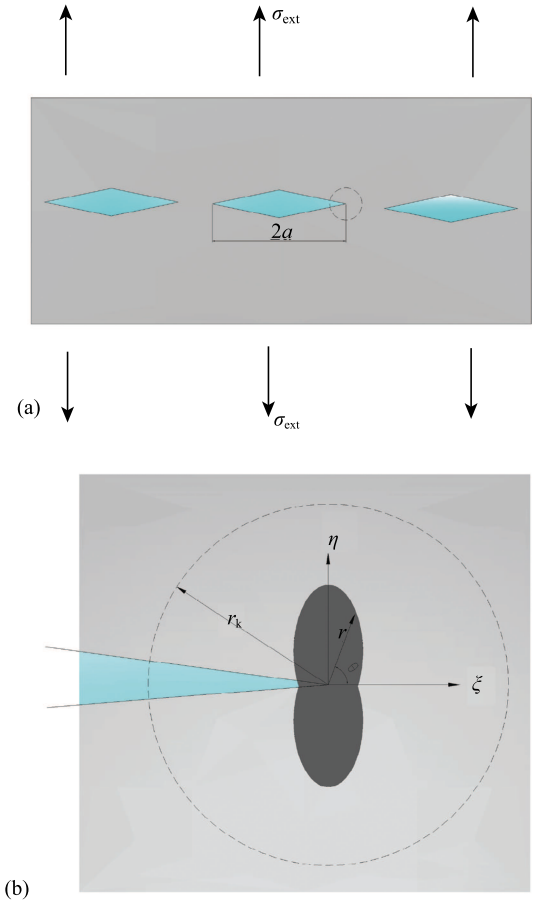

Fig. 4. (color online) (a) Some microcracks of length $2a$, which are surrounded by hydrogen/helium, with an external tensile stress load $\sigma_{\rm ext}$. (b) an enlargement of the near-field region of radius $r_{\rm K}$ which is located to the right of the crack; ξ, η, ζ is a local cartesian system; the black areas represent the plastic zone, which are indicated by cylindrical polar coordinates (r,θ).

$$\left\{\begin{array}{c}\sigma_1\\ \sigma_2\\ \sigma_3\end{array}\right\}=\frac{K_{\rm I}}{\sqrt{2\pi r}}\cos\frac{\theta}{2}\left\{\begin{array}{c}1+\sin\theta/2\\ 1-\sin\theta/2\\ 2\nu\end{array}\right\}, \tag{10}$$

where $r_{\rm p}(\theta)<r<r_{\rm K}\ll a,-\pi<\theta<\pi,v$ is the Poisson ratio, and $K_{\rm I}$ is the stress-intensity factor.

$$K_{\rm I}=(\sigma_{\rm ext}+p_{\rm int})\sqrt{\pi a}. \tag{11}$$

Here, $p_{\rm int}$ denotes the partial pressure of an internal atmosphere of molecular hydrogen/helium in local equilibrium with atomically dissolved hydrogen/helium encompassing the crack. $\sigma_{\rm F}$ means uniaxial tensile stress. When $\sigma_{\rm ext}+p_{\rm int}\ll\sigma_{\rm F}$, according to the von Mises yield criterion,

$$(\sigma_1-\sigma_2)^2+(\sigma_2-\sigma_3)^2+(\sigma_3-\sigma_1)^2=2\sigma_{\rm F}^2, \tag{12}$$

the contour equation of the plastic zone is described by Eq. (13):

$$r_{\rm p}(\theta)=\frac{K_{\rm I}^2}{2\pi\sigma_{\rm F}^2}\cos^2\left((1-2v)^2+3\sin^2\frac{\theta}{2}\right). \tag{13}$$

When θ=0, Eq. (13) describes the lateral extent of the plastic zone,

$$r_{\rm p}^*=\frac{1}{2\pi}\left((1-2v)\frac{K_{\rm I}}{\sigma_{\rm F}}\right)^2. \tag{14}$$

The near-field region and the plastic zone of the crack are illustrated in Fig. 4(b).

The interaction between the hydrogen/helium atom and the crack-tip stress field can be written as

$$W=-\frac{1}{3}(\sigma_1+\sigma_2+\sigma_3)\Delta V. \tag{15}$$

Here, ΔV denotes the relaxation volume, originating from the strain field around the hydrogen/helium defect and the action of image forces due to the surfaces of the plate, and is related to F_0 via Hooke's law,

$$\Delta V=\frac{({\rm tr}F_0)}{3B}. \tag{16}$$

B is the bulk modulus. In this work, the hydrogen/helium relaxation volume is calculated using the Vienna ab initio Simulation Package VASP [18]. The results are shown in Table 2. Substituting Eq. (10) into Eq. (15), we obtain the interaction between the hydrogen/helium atom and the crack-tip stress field

$$W=-\sqrt{\frac{2}{9\pi r}}(1+v)K_{\rm I}\Delta V\cos\frac{\theta}{2}. \tag{17}$$

When $r=r_{\rm p}^*,\theta=0$, Eq. (18) adopts its minimum,

$$W_{\rm min}=-\frac{2}{3}\left(\frac{1+v}{1-2v}\right)\sigma_{\rm F}\Delta V. \tag{18}$$

From Eq. (18), it is obvious that the minimum of the interaction $W_{\rm min}$ is independent of the stress intensity factor $K_{\rm I}$.

The Bragg-Williams model can describe the concentration of mutually non-interacting hydrogen/helium atoms, and it is impossible that two solute atoms can occupy one site because of the short-range repulsion. The maximum hydrogen/helium concentration due to stress-driver hydrogen/helium accumulation in front of the crack-tips follows from the Fermi-Dirac distribution [19]

$$c_{\rm max}=\frac{1}{\exp\left(\dfrac{W_{\rm min}-G_0}{k_{\rm B}T}\right)+1}, \tag{19}$$

where the minimum energy $W_{\rm min}$ is given by Eq. (18) and G_0 is the local chemical potential, given by Eq. (20):

$$G_0=k_{\rm B}T\log\left(\frac{c_0}{1-c_0}\right). \tag{20}$$

If $W_{\rm min}-G_0\gg k_{\rm B}T>0$ and $0<c_0\ll1$, Eq. (20) can simplify to the Boltzmann distribution

$$c_{\rm max}\approx c_0\exp\left(-\frac{W_{\rm min}}{k_{\rm B}T}\right). \tag{21}$$

According to Eq. (20), the maximum hydrogen/helium concentration near the tips of a microcrack are shown in Fig. 5.

Comparing Fig. 2 and Fig. 5 we note that the maximum hydrogen concentration exceeds the hydrogen background concentration by about 1.2–1.8 times and the maximum helium concentration exceeds the helium background concentration by about 2–4 times. Figure 6 shows the ratio of the maximum hydrogen/helium concentration and the hydrogen/helium background concentration with the uniaxial tensile flow stress, according to Eq. (19) and Eq. (5).

The uniaxial tensile flow of tungsten between 0℃ and 500℃ can be described by the linear function Eq. (21), giving

$$\sigma_{\rm F}=736.5-0.5T\ \ (273\ {\rm K}\leqslant T\leqslant 573\ {\rm K}). \tag{22}$$

Finally, combining Eq. (18)–(20) and Eq. (22), we can get Fig. 7, which shows the maximum hydrogen/helium concentration near the tips of a microcrack in tungsten, as a function of the temperature, at two values of the transfer length, when the value of the plate half-thickness

is 14 mm. From Fig. 7, we note that the maximum hydrogen/helium concentration decreases with the increase of temperature.

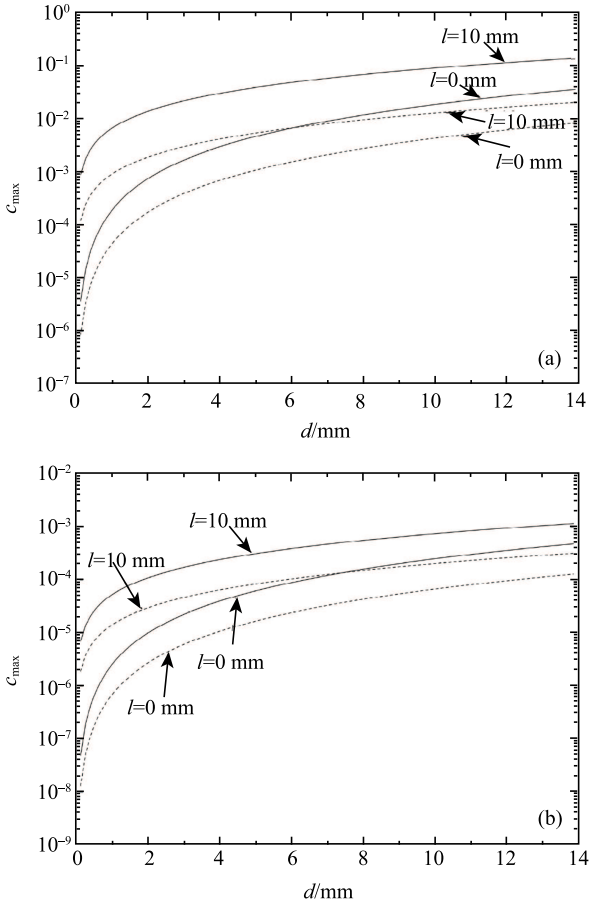

Fig. 5. The maximum hydrogen/helium concentration near the tips of a crack in the center of the tungsten plate, as a function of d, (the plate half-thickness), at two different temperature of 100℃ (solid line) and 300℃ (dotted line), for different values of the transfer length l, for (a) maximum hydrogen concentration; (b) maximum helium concentration.

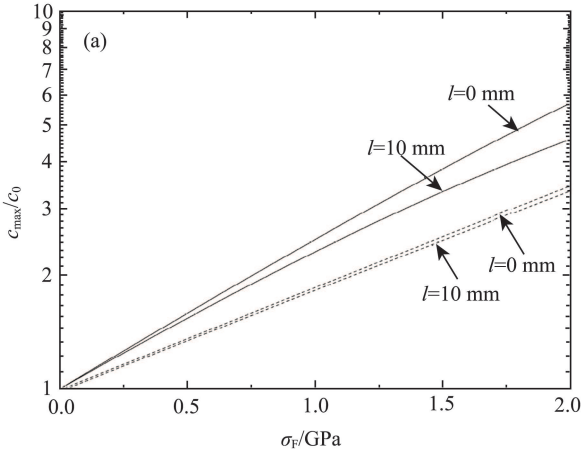

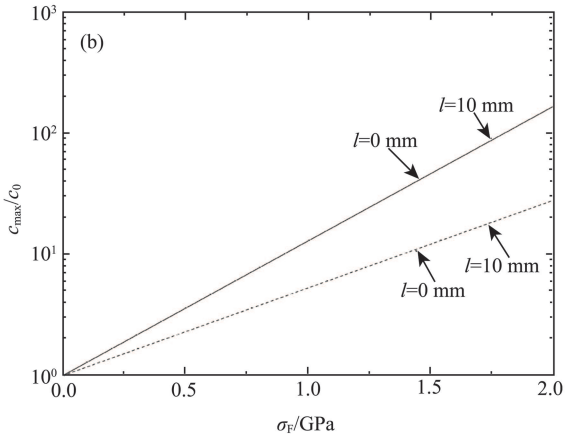

Fig. 6. The ratio of the maximum hydrogen/helium concentration and the hydrogen/helium background concentration in tungsten, as a function of the uniaxial tensile flow stress, at two different temperatures, 100℃ (solid line) and 300℃ (dotted line), for different values of the transfer length l, for (a), the $c_{\max}/c_0$ of hydrogen; (b), the $c_{\max}/c_0$ of helium.

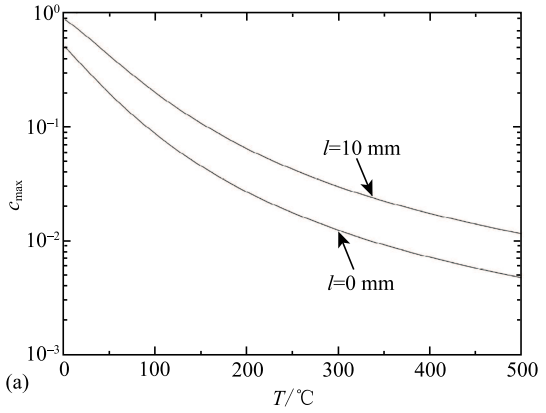

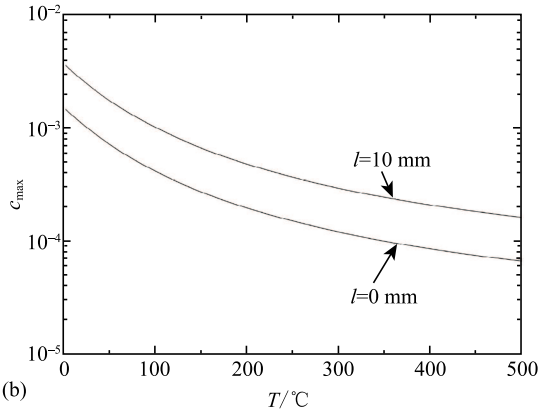

Fig. 7. The maximum hydrogen/helium concentration near the tips of a crack in the center of the tungsten plate, as a function of the temperature, at two values of the transfer length (l=10 mm, l=0 mm) and d=14 mm, for (a) maximum hydrogen concentration; (b) maximum helium concentration.

3 Conclusions

The hydrogen/helium concentration is one of the important factors in causing hydrogen/helium degradation in a spallation target. In this work we applied a theoretical model to calculate the hydrogen/helium background concentration and their enhancement near cracks in tungsten irradiated by 1.6 GeV protons. For the CSNS target, the half-thickness of the tungsten target plate with the highest operating temperature is d=14 mm and its operating temperature is below 300℃. According to the model and the parameters described above we can get the following results:

1) The range of the hydrogen background concentration in the tungsten target is 2.1×10^{-2}–1.2×10^{-1}; the helium background concentration is 1.6×10^{-4}–2.9×10^{-4}.

2) The range of the relaxation time of hydrogen in the tungsten target is 10 days–50 days, and the helium is 7 hours–13 hours.

3) The range of the maximum hydrogen concentration near the tips of cracks in a tungsten target is 3.0×10^{-2}–2×10^{-1}, which exceeds the hydrogen background concentration by 1.2–1.8 times; the maximum helium concentration range near the tips of cracks in a tungsten target is 3.0×10^{-4}–1.2×10^{-3}, which exceed the hydrogen background concentration by 2–4 times.

4) In a tungsten target, the hydrogen/helium concentration increases with the increase of the transfer length across the surfaces of the plate l and the maximum hydrogen/helium concentration decreases with the increase of temperature.

5) For 0.3 mm-thick tantalum cladding, we find that the maximum hydrogen concentration near the tips of cracks ranges from 3.73×10^{-5} to 5.25×10^{-4}.

References

1 FangWei Wang, TianJiao Liang, Wen Yin et al, Science China Physics, Mechanics & Astronomy, **56**:2410 (2013)
2 R. L. Klueh, N.Hashimoto, M. A. Sokolov, K. Shiba et al, J. Nucl. Mater, **357**:156 (2006)
3 R. L. Klueh, N. Hashimoto, M. A. Sokolov et al, J. Nucl. Mater, **357**:169 (2006)
4 Charlotte S. Becquart and Christophe Domain, Physical Review Lett, **97**: 196402 (2006)
5 H. Trinkaus and B. N. Singh, J. Nucl. Mater, **323** :229 (2003)
6 H. Amara, C. C. Fu, F. Soisson, and P. Maugis, Physical Review B, **81** : 174101 (2010)
7 Peng Zhang, Yong Lu, Chao-Hui He, and Ping Zhang, J. Nucl. Mater, **418**:143 (2011)
8 Fasso A, Ferrari A, Ranft J, and Sala P R, *FLUKA: A Multi-Particle Transport Code*. CERN 2005-10, INFN/TC 05/11, SLAC-R-773. 2005
9 Battistoni G, Muraro S, Sala P R, Cerutti F, Ferrari A, Roesler S, Fasso A, and Ranft J, The FLUKA Code: Description and Benchmarking. In *Proceedings of the Hadronic Shower Simulation Workshop 2006*, edited by Vol,896, Albrow M, Raja R Fermilab 6-8September 2006, *AIP Conference Proceeding*, 2007, p.31-49
10 Yi-Nan Liu, Tiefeng Wu, Yi Yu et al, J. Nucl. Mater, **455**:676 (2014)
11 Xiaolin Shu, Peng Tao, Xiaochun Li, Yi Yu, Nucl. Instrum. Methods B, **303**:84 (2013)
12 S. L. Green, W. V. Green, F. H. Hegedus, M. Victoria, J. Nucl. Mater, **155-157:** 1350 (1988)
13 W. Yin, Q. Z. Yu, Y. L. Lu et al, J. Nucl. Mater, **431**: 39 (2012)
14 H. Rauh, R. Bullough, J. R. Matthews, Philos. Mag. A, **65**: 53 (1992)
15 J. D. Hobson, J. Iron Steel Inst, **191**: 342 (1959)
16 H. Rauh, H. Ullmaier, J. Nucl. Mater, **295:** 109 (2001)
17 D. Broek, *Elementary Engineering Fracture Mechanics*(Fourth Edition, Kluwer Academic Publishers, 1991), p.92-99
18 G. Kresse and D. Joubert, Phys. Rev. B, **47**: 558(1993); **49**:14251 (1994)
19 A. P. Sutton, R. W. Balluffi, *Interfaces in Crystalline Materials* (Oxford University Press, 2006), p.436